ELSEVIER

Journal of Nuclear Materials 313–316 (2003) 813–819

journal of nuclear materials

www.elsevier.com/locate/jnucmat

Intermittent convection in the boundary of DIII-D

J.A. Boedo [a,*], D.L. Rudakov [a], R.J. Colchin [b], R.A. Moyer [a], S. Krasheninnikov [a], D.G. Whyte [a], G.R. McKee [c], G. Porter [f], M.J. Schaffer [d], P.C. Stangeby [e], W.P. West [d], S.L. Allen [f], A.W. Leonard [d]

[a] *San Diego Energy Research Center, University of California, 9500 Gilman Drive, La Jolla, CA 92093, USA*
[b] *Oak Ridge National Laboratory, P.O. Box 2008, Oak Ridge, TN 37831, USA*
[c] *University of Wisconsin, 1500 Engineering Drive, Madison, WI, 53706, USA*
[d] *General Atomics, P.O. Box 85608, San Diego, CA 92186-5608, USA*
[e] *Institute for Aerospace Studies, University of Toronto, 4925 Dufferin St., Toronto, Canada, M3H 5T6*
[f] *Lawrence Livermore National Laboratory, P.O. Box 808, Livermore, CA 94551, USA*

Abstract

Intermittent plasma objects (IPOs) featuring higher pressure than the surrounding plasma, and responsible for ~50% of the $E \times B_T$ radial transport, are observed in the scrape-off layer (SOL) and edge of the DIII-D tokamak. The skewness (i.e., asymmetry of fluctuations from the average) of probe and BES intermittent data suggest IPO formation at or near the last closed flux surface (LCFS) and the existence of hole–IPO pairs. The particle content of the IPOs at the LCFS is linearly dependent on the discharge density, however, when normalized to the local averaged density, it is fairly insensitive to density variations. It is also shown that the IPOs thermalize with the background plasma within 1 cm of the LCFS. The IPOs appear in the SOL of both *L* and *H* mode discharges carrying ~50% of the total SOL radial $E \times B_T$ transport at all radii. However, the total flux and the IPO contribution, are highly reduced in *H*-mode conditions due to the increased confinement.

Keywords: Transport; Intermittency; SOL; Tokamak

1. Introduction

A magnetic divertor [1] in a tokamak provides heat and particle exhaust and shields the main plasma from impurity contamination. Heat and particles are transported from the plasma core to the edge and scrape-off layer (SOL) plasma, where they are, in turn, conducted and convected to the divertor, which is optimized to reduce structural damage and impurity release. The balance between parallel and perpendicular transport results in a SOL which is thin compared to its length [1] and the observed SOL density profiles are mostly exponential [2] with short (1–3 cm) decay lengths. However, there is ample [3–5] evidence that the SOL density profiles are sometimes wider than usual and non-exponential and flat far away from the last closed flux surface (LCFS), suggesting that perpendicular transport in these conditions can be larger than expected.

A candidate for the additional edge/SOL transport, intermittency in the fluctuations corresponding to a significant number of events above the standard deviation, has been documented extensively in linear devices [6,7] stellarators [8] and tokamaks [9–11] and its statistical properties examined [12] via a probability distribution function (PDF) [13]. The essential result is that the fluctuations depart from Gaussian behavior,

* Corresponding author. Address: C/o General Atomics, P.O. Box 85608, San Diego, CA 92186-9784, USA. Tel.: +1-858 455 2832; fax: +1-858 534 7711.
E-mail address: jboedo@ucsd.edu (J.A. Boedo).

0022-3115/03/$ - see front matter
PII: S0022-3115(02)01443-5

featuring skewness [13] and kurtosis [13] that correspond to the presence of a significant number of events above the standard deviation. Furthermore, it has been proven in tokamaks (JET) and stellarators [14] (ATF, W7-AS) that the statistical properties of the fluctuations are similar and near-Gaussian in the shear layer while deviating from Gaussian into the edge or the SOL [14]. The intermittent events have been characterized using conditional averaging tools in both linear devices [6,7] and tokamaks [15,16] with the result that structures propagating radially are responsible for much of the radial transport. Recent work in the CASTOR tokamak [17], using conditional averaging reported intermittent coherent structures propagating radially and poloidally in the SOL. Comparative work at the devices TJ-I and TJ-IU, concluded that intermittency bears a substantial part of the transport and most importantly, that the various properties of the intermittency (power spectra, PDF moments, etc.) are self-similar in tokamaks and torsatrons. Recent work in the JET tokamak [18] focused on the power spectra of the fluctuations, demonstrating that decay as $1/f$ was localized in the spectral region where intermittent (or bursty) transport is dominant and interpreting the result as an indication of closeness to instability thresholds. Therefore, the universality of intermittency and the concomitant fast convective transport has been long established [6,8, 19,20] and there is an extensive body of work imaging the edge of various devices with fast cameras [21,22] with the result that moving plasma filaments exist in the edge/SOL.

This paper builds on recent work [16] demonstrating the existence of intermittency in the DIII-D boundary and characterizing it. We now present results from various diagnostics strongly indicating that the origin of the intermittency phenomena is at or near the LCFS. Furthermore we present scaling of the magnitude of the density perturbations with density in L-mode and show that the intermittent plasma objects (IPOs) quickly thermalize with the background plasma. The role of the IPOs on radial transport is a constant fraction of the total on all conditions and is quite significant at nearly 50%.

2. Experimental setup

The experiments were carried out on the DIII-D tokamak [23] in a variety of discharges with plasma current $I_p = 1.0$ MA and toroidal field of $B_T = 2.0$ T at the axis, $R = 1.7$ m. For completeness, a brief survey of discharges with neutral beam heating power of up to 2 MW, featuring both low (L) and high (H) confinement modes, with double- and single-null divertor geometry (at the bottom of the vacuum vessel) and with standard and reversed B_T directions were investigated. Otherwise

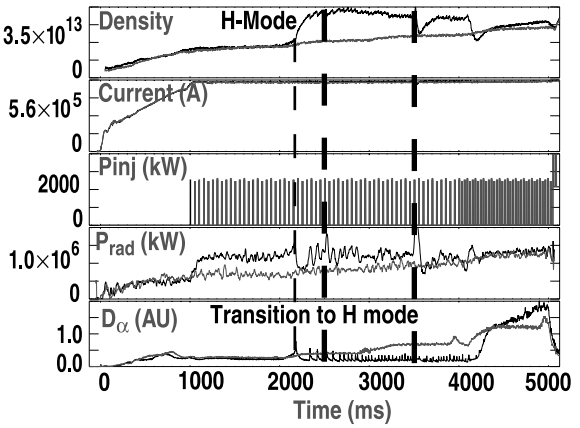

Fig. 1. Time evolution of two discharges in DIII-D showing from top to bottom, density, plasma current, injected power, radiated power and D_α signals. The transition to H-mode occurs at 2.15 s in one of the discharges. The probe is inserted at the times marked by the two thick vertical lines.

identical H- and L-mode discharges, shown in Fig. 1, were analyzed in particular detail for comparative studies. In some discharges, the density was increased in

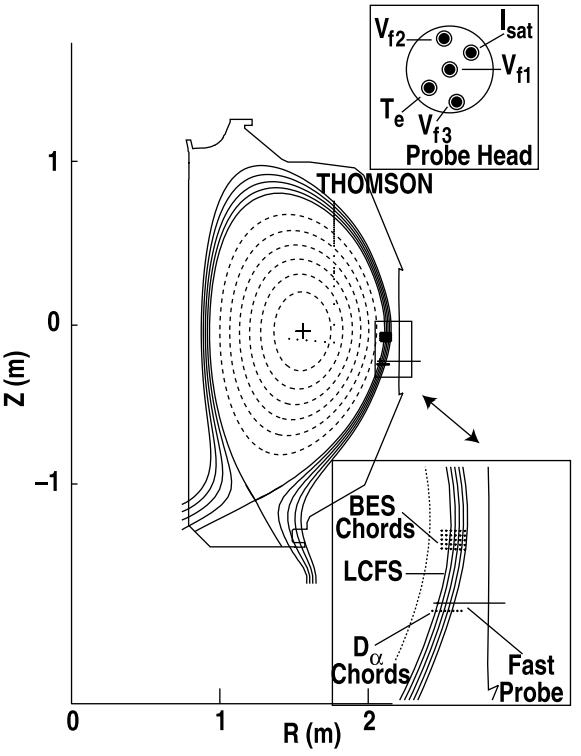

Fig. 2. Poloidal cut of DIII-D showing the magnetic geometry and some relevant diagnostics. Two insets show (top) the scanning probe tip geometry and (bottom) the BES diagnostic geometry.

a stepwise manner from $\langle n_e \rangle / n_{GW} = 0.26$ to 0.5, as shown in Figs. 1 and 3, and the reciprocating probe at the midplane (Fig. 2) was inserted at various times, illustrated by the vertical lines, to assure coverage at various densities.

The principal measurements were made by a fast scanning probe array [24] featuring five tips (Fig. 2 upper inset) that sense probe current I, ion saturation current I_{sat}, given by the expression $I_{sat} = (1/2) \times A_{pr} e n_e c_s = (1/2) A_{pr} e n_e [k(T_e + T_i)/m_i]^{1/2}$, ($T_e$ and T_i are the ion and electron temperatures respectively, A_{pr} is the tip area and n_e is the electron density) and floating potential, Φ_f. These measurements were used to infer electron temperature, T_e, by using the harmonic method [25], the electron density, n_e, by using the equation above. The probe scans horizontally from the outside wall in approximately 250 ms along the path indicated in Fig. 2. The D_α sensor array, also shown in Fig. 2, provided independent, radially resolved intermittent signals. The beam emission spectroscopy (BES) system, configured as a 5×6 fiber array as seen in Fig. 2, was located at the edge of the plasma in the midplane to provide fast (1 μs) 2-D imaging of the density. The measurements can be mapped onto the magnetic surfaces, displayed in Fig. 2, calculated by the toroidal equilibrium fitting code EFIT [26].

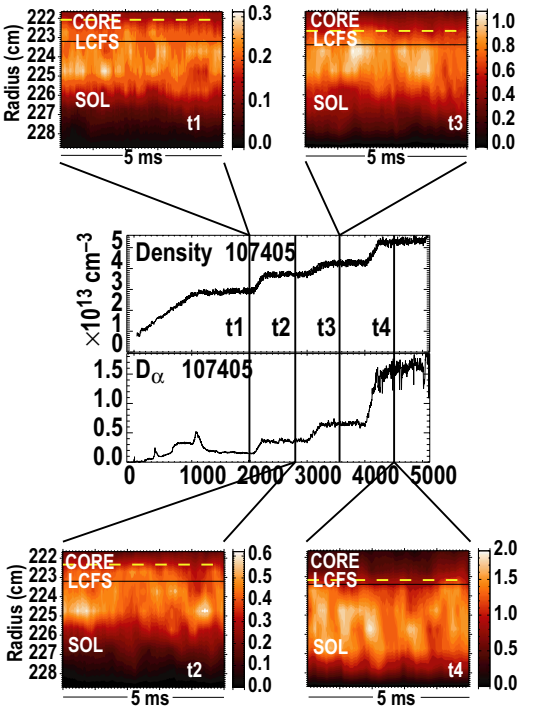

Fig. 3. The time evolution of the L-mode discharge showing the density steps with $\langle n_e \rangle / n_{GW}$ varying from 0.27 to 0.5. Inserted 2-D plots show the time evolution of the D_α radial array signals in a 5 ms scale showing the intermittency and its variation with plasma averaged density.

3. Results: general description of the intermittency

Appreciable intermittency is evident in many edge diagnostics [16] and the intermittent objects appear at a rate of 1×10^3 to 4×10^3 s^{-1} and, although correlation of the large excursions can be observed by eye among all the traces, conditional averaging tools, introduced in the TEXT tokamak by Filippas et al. [15] and later in linear devices [6] and other tokamaks [8], were used to quantify the observations. A 2.5 × rms-level threshold was routinely used to discriminate the intermittent events in n_e, T_e and I_{sat} probe data, which are then clipped for 100 μs about the maximum of each event, accumulated and then averaged. The existence of an event in a signal can be used as the condition to clip time slices in other signals at the same time slices to observe correlations.

A convenient way of visualizing the intermittency is shown in Fig. 3, where data from the radial D_α array (Fig. 2) is plotted in 2-D with the ordinate corresponding to the radial direction (top is the core, bottom the SOL) and the abscissa to time. The data, which is not shown in the same scale for clarity, displays structures that appear intermittently, travel radially and poloidally and then dissipate. Notice that the structures are born in a region (marked with a dashed line) slightly inside the LCFS (marked with a solid line) *only and do not come from deeper in the plasma core.* The intensity of the intermittent Da signal increases linearly with density (note scale). Data from the BES diagnostic, which measures density in a 2-D array covering a 6 cm × 5 cm region at the edge plasma (Fig. 2) with 1 μs resolution, was also used to visualize the data. Two frames taken at an arbitrary time t_0 and 6 μs later ($t_0 + 6$ μs) are shown in Fig. 4, indicating the LCFS is indicated by a solid vertical line. The radial motion of a positive density feature, marked by a dashed circle in both frames, is indicated by vertical dashed lines. Notice that the object has a spatial extent of roughly 2 cm × 2 cm. From the two frames it is clear that the object is moving poloidally and radially with speeds that can be easily estimated at $V_\theta = 5$ km/s and $V_r = 1.5$ km/s which compare well to probe data.

The intermittency causes asymmetry on statistics of the various signals introducing a deviation from Gaussian behavior, in both L- and H-mode, that is measured as skewness (i.e., positive n_e bursts appear as positive skewness) [13] of ~1 in the I_{sat} signal at the SOL, as shown in Fig. 5(a). Similar results are obtained from BES [27,28] data, shown in Fig. 5(b). It is crucial to notice that the skewness changes sign at or near the LCFS, within the error bars of EFIT, indicating that negative events are present, corresponding to drops in the density signal from its average level.

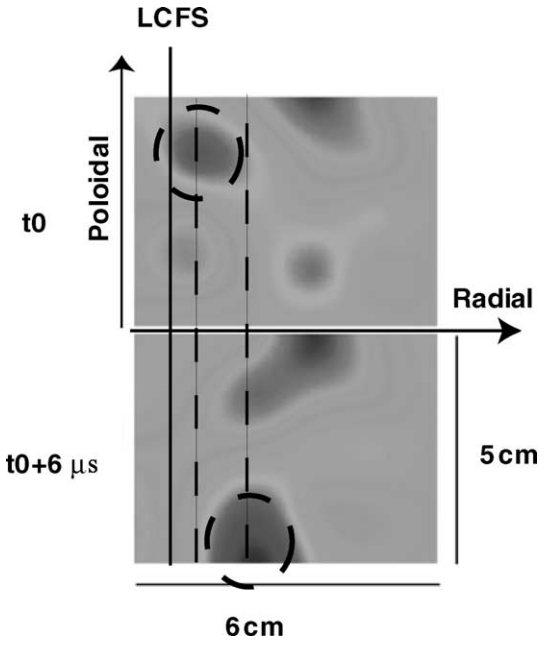

Fig. 4. Two frames from BES showing 2-D density plots. There is a time difference of 6 μs between frames. A particular structure is marked with a dashed circle, and shown in both frames, clearly highlighting poloidal and radial motion.

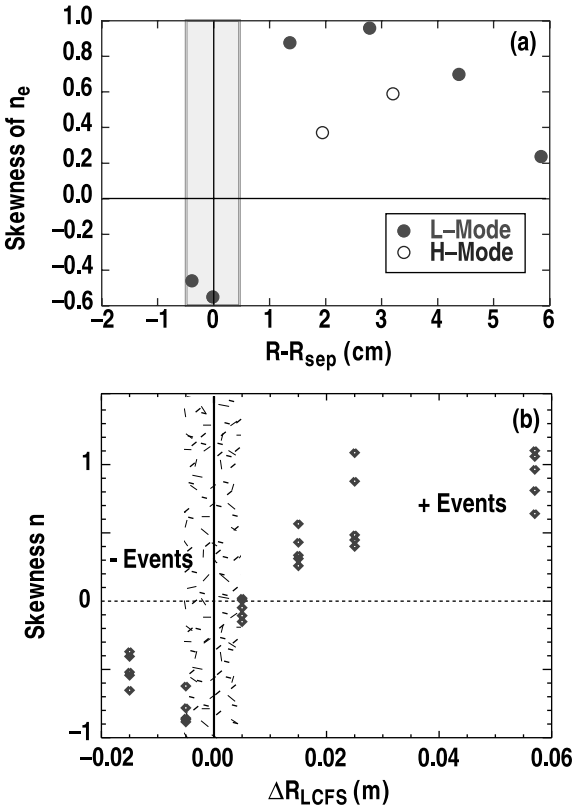

Fig. 5. The skewness of: (a) the I_{sat} signal, and (b) the BES signal is shown for L-mode (open circles) and H-mode (solid circles) discharge conditions, showing marked deviation from Gaussian behavior. The skewnes reverses roughly at the LCFS.

Conditional averaging performed on the probe's density data averaged over 5 ms (threshold at 2.5 × rms level) near the LCFS, and shown in Fig. 6 for discharges with $\langle n_e \rangle / n_{GW} = 0.26$ and 0.5, confirm the presence of *both* positive and negative events. It can be seen that the positive and negative (hole) IPOs are comparable in size, suggesting that a local relaxation in the density profile is the source of the positive IPOs, and in agreement with the D_α array shown in Fig. 3.

Conditional averaging of probe signals as a function of radius produces profiles of the typical IPO, for L and H-mode. The results for density are shown in Fig. 7(a) and (b) for L- and H-mode discharges, in the same scale for ease of comparison, by superimposing traces from various radii and indicating (arrow) the direction of increasing radius. Three properties of the data are apparent: (1) the density excursion is 2–3 times the background density, (2) the amplitude of the pulses for similar radius is much larger for L-mode conditions than for H-mode conditions, and (3) the amplitude of the pulses decays rapidly with radius.

Since the interaction of the plasma with the far wall has been reported to increase with density [29], and the IPOs can provide a mechanism for fast convection of particles, it is interesting to explore the scaling of the amplitude of the density IPOs with core density. Radial profiles of the IPO peak density/temperature, and the averaged density/temperature profiles, are shown in Fig.

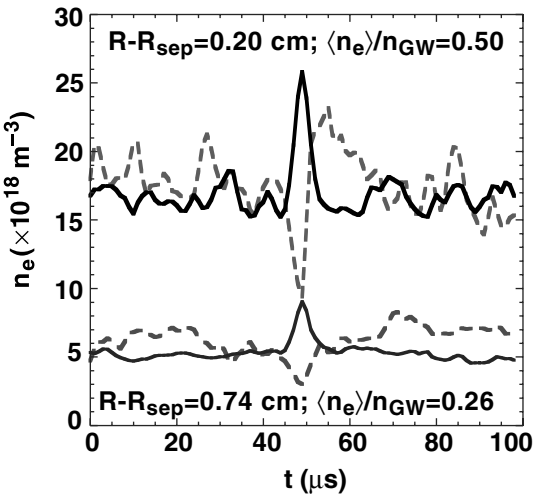

Fig. 6. Conditional averaging of the probe density signals near the LCFS for $\langle n_e \rangle / n_{GW} = 0.27$ and 0.5 indicate the existence of density holes concomitantly with IPOs in that region. This data supports the paradigm of the IPO creation near the LCFS.

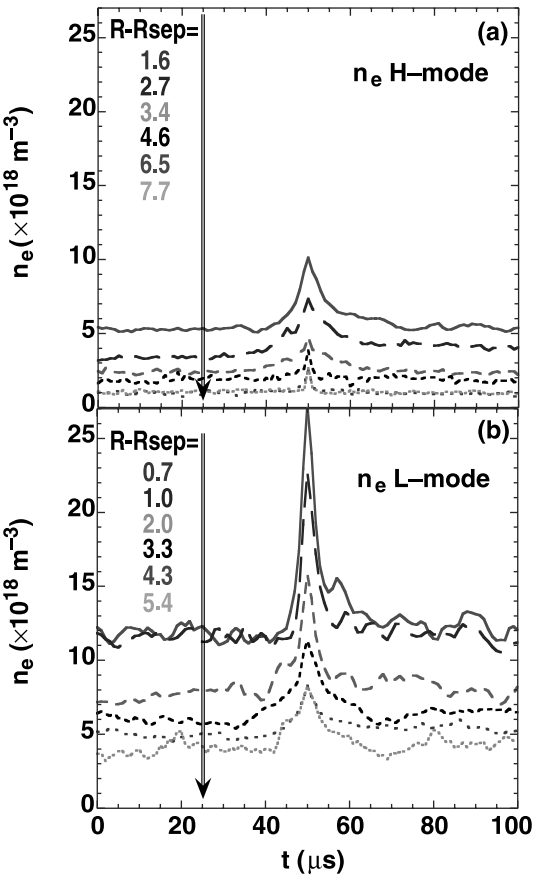

Fig. 7. Conditional averaging results showing the density pulses for L- and H-mode conditions. Data from different radii are superimposed, those from the LCFS at the top and those from the far SOL at the bottom, as the arrows and labels indicate. Density pulses in L-mode are larger than in H-mode. Profiles are shown in Fig. 8.

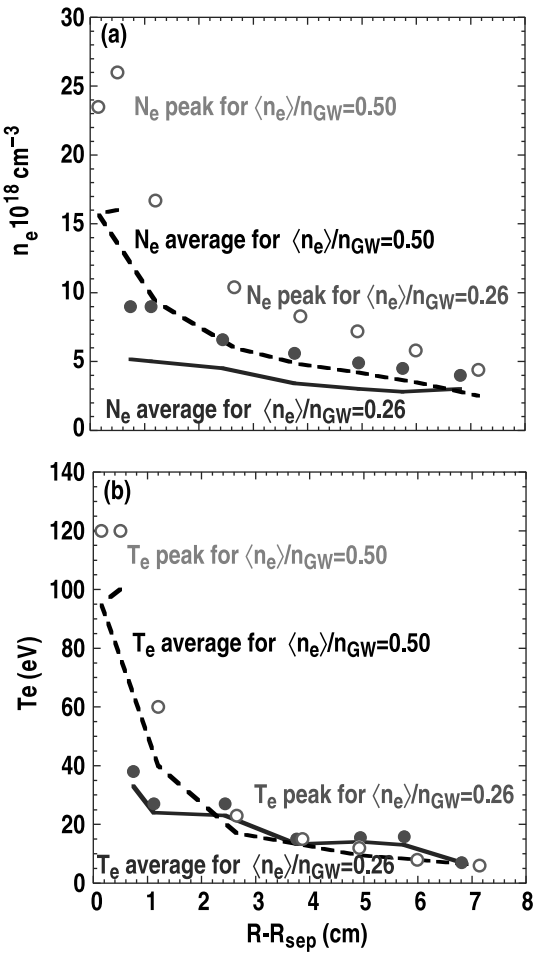

Fig. 8. Radial profiles of (a) the IPO peak density (from conditional averaging) and the average profile and (b) the IPO peak temperature and the average profile for low and high density cases ($\langle n_e\rangle/n_{GW} = 0.27$ and 0.5). The peak IPO density decays with the same scale length as the background profile while the peak temperature decays much faster.

8(a) and (b) for L-mode discharges with $\langle n_e\rangle/n_{GW} = 0.26$ and 0.5. It can be noted in Fig. 8(a) that the peak IPO density is about 70% of the background density and both decay quickly with radius with a decay length, *Ln*, of 2.7 cm. Quite different behavior is seen on the temperature, obtained from a fast T_e diagnostic [30], where the IPO peak temperature decays to that of the background profile within 1 cm. Therefore, the IPOs quickly thermalize with the background.

The relative importance of the IPO density can be evaluated as a function of $\langle n_e\rangle/n_{GW}$ by calculating $(n_e^{peak} - \langle n_e^{aver}\rangle/\langle n_e^{aver}\rangle)$ for various radii in the SOL, shown in Fig. 9. The outcome is quite surprising, despite the fact that the particle content (or density excursion) of the IPOs increases with density (as seen in Fig. 3 and Fig. 8(a)), it is clear that the IPOs relative contribution to the density is fairly constant with radius and density at about 50–70%. This results suggest a scaling of the IPO intensity with transport or vice versa.

Evaluation of the total particle flux convected by these events is of utmost importance to assess their relevance to the radial transport. The flux can be calculated as $\Gamma_{int} = n_e(E_\theta \times B/B_2)$ and the result can be seen in Fig. 10 for L- and H-mode conditions and in the same scale. Three properties are again quite apparent, (1) the flux excursion is four times the background, (2) the flux for similar radius is much larger for L-mode conditions than for H-mode conditions, and (3) the flux decays rapidly with radius. As reported earlier [16], it is found that $\Gamma_{int}/\Gamma_{total} = \langle I_{sat}E_\theta\rangle_{intermittent}/\langle I_{sat}E_\theta\rangle_{total}$, obtained in L- and H-mode, is roughly 50% at all radii. Although the relative relevance of intermittency is unchanged with radius, its absolute amplitude decays rapidly with radius.

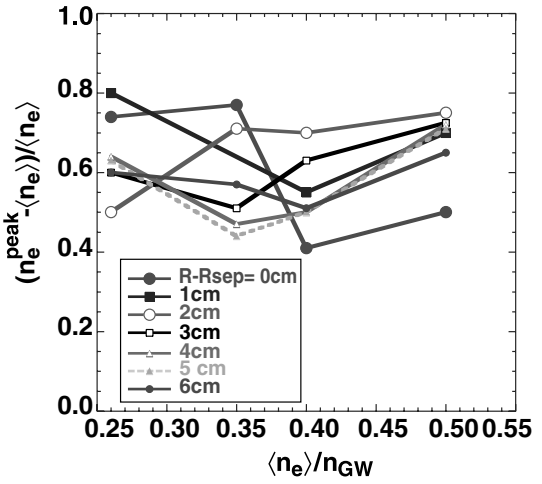

Fig. 9. The normalized intensity of the IPO density for various radius is features independence from the discharge density (in $\langle n_e \rangle / n_{GW}$ units).

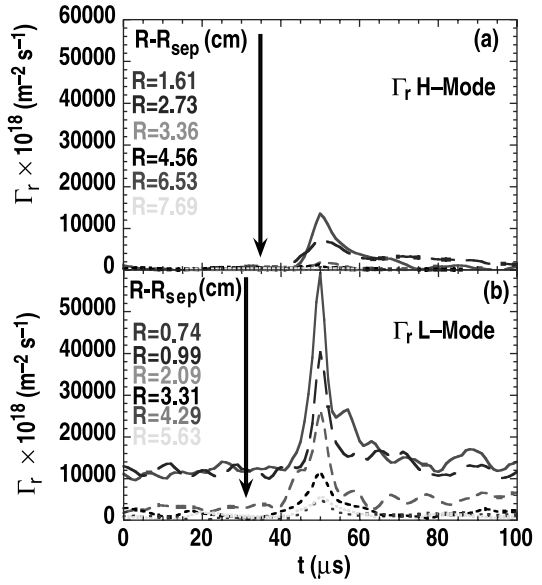

Fig. 10. Conditional averaging results showing the intermittent particle flux for L- and H-mode conditions. Data from different radii are superimposed, those from the LCFS at the top and those from the far SOL at the bottom, as the arrows indicate. The corresponding radii are indicated. Particle flux in L-mode is larger than in H-mode.

However, the quick reduction in the amplitude of the bursts and concomitant fast decay of the density profiles is not in contradiction with a strong particle sink in the divertor for the conditions shown. The decay of the IPO, considered as elongated structures along the magnetic field, density and temperature has been analytically predicted in recent work [31,32] to be

$$n(r,t) = n(r)/(1 + t/\tau_T)^{2\alpha/\alpha_T} \text{ and}$$
$$T(t) = T_0/(1 + t/\tau_T)^2, \quad (1)$$

where $\alpha_T = \alpha S_E$; $\tau_T = 2/(\alpha_T T_0^{1/2})$, α measures the net parallel current to the divertor plates, S_E is the sheath energy transmission factor and T_0 is the temperature of the IPO as it detaches from the LCFS. Since $2\alpha/\alpha_T = 2/S_E \ll 1$ and thus much smaller than the temperature exponent, the temperature decays much more rapidly then the density, just as observed in the experiment (Fig. 8(a) and (b)).

4. Conclusions

Intermittency in the boundary of the DIII-D tokamak during L- and H-mode discharges is present, as indicated by data from various diagnostics. The H-mode data for this work has been evaluated between ELMs. The data shows that structures featuring higher density and temperature than the surrounding plasma seem to originate at or near the LCFS and travel radially in the SOL, transporting particle and energy. Although the amplitude of the IPOs in L-mode increases with density at the LCFS, they carry a fairly constant fraction (50–70%) of the local density at all radii and densities measured, Furthermore, the IPOs feature higher temperature than the background at the LCFS, but they become thermalized within a short distance of the LCFS, in agreement with analytical predictions. In L-mode, the IPO phenomena is important to determine the structure of the SOL and it determines an somewhat enhanced plasma–wall contact. However, the presence of ELMs in H-mode, carrying more energy and particles than the IPOs, transiently dominates the structure of the SOL and the plasma–wall interaction.

Acknowledgements

Work supported by the US Department of Energy under Grants DE-FG03-95ER54294, DE-FG03-96ER54373, Contracts DE-AC03-99ER54463, DE-AC05-00OR22725, and W-7405-ENG-48. Discussions with D. D'Ippolito are acknowledged.

References

[1] P.C. Stangeby, The Plasma Boundary of Magnetic Fusion Devices, IoP, 2000, p. 46.
[2] P.C. Stangeby, G. McCracken, Nucl. Fusion 30 (7) (1990).
[3] J.A. Boedo, D. Gray, et al., Rev. Sci. Instrum. 69 (7) (1998) 2663.
[4] B. LaBombard, M.V. Umansky, R.L. Boivin, J.A. Goetz, et al., Nucl. Fusion 40 (12) (2000) 2041.
[5] M.R. Wade et al., J. Nucl. Mater. 266–269 (1999) 44.

[6] A.H. Nielsen, H.L. Pecsell, J. Juul Rasmussen, Phys. Plasmas 3 (5) (1996) 1530.
[7] R.D. Lehmer, PhD thesis, University of California Los Angeles, UCSD-ENG-032, 1996.
[8] E. Sanchez, C. Hidalgo, C. Riccardi, J. Bleuel, B. Carreras, D.E. Newman, et al., Phys. Plasmas 7 (5) (2000) 1408.
[9] B.K. Joseph, R. Jha, P.K. Kaw, S.K. Mattov, et al., Phys. Plasmas 4 (1997) 4292.
[10] R.A. Moyer, R.D. Lehmer, T.E. Evans, et al., Plasma Phys. Contr. Fusion 38 (1996) 1273.
[11] R. Jha, Y.C. Saxena, Phys. Plasmas 3 (8) (1996) 2979.
[12] B. Carreras et al., Phys. Plasmas 7 (2000) 3278.
[13] W. Press, S. Teukolsky, W. Vettering, B. Flannery, Numerical Recipes in Fortran, Cambridge University Press, Cambridge, 1986, p. 606.
[14] E. Sanchez, C. Hidalgo, D. Lopez-Bruna, I. Garcia-Cortes, R. Balbin, et al., Phys. Plas. 7 (5) (2000) 1408.
[15] A.V. Filippas, R.D. Bengtson, G.X. Li, M. Meier Ritz, Ch.P. Ritz, et al., Phys. Plasmas 2 (1995) 839.
[16] J.A. Boedo, D. Rudakov, R. Moyer, et al., Phys. Plasmas 8 (2001) 4826.
[17] J. Soteckel, M.V. Heller, J. Petrzilka, et al., Phys. Plasmas 6 (3) (1999) 846.
[18] I. Garcia-Cortes, R. Balbin, A. Loarte, J. Bleuel, et al., Plas. Phys. Contr. Fusion 42 (2000) 389.
[19] G. Antar, S. Krasheninnikov, et al., Phys. Rev. Lett. 87 (2001) 650.
[20] G. Antar, P. Devynck, X. Garbet, S. Luckhardt, Phys. Plasmas 8 (5) (2001) 1612.
[21] S.J. Zweben, S.S. Medley, Phys. Fluids B 1 (1989) 2058.
[22] R. Maqueda, G. Wurden, S. Zweben, et al., Rev. Sci. Instrum. 72 (2002) 931.
[23] J.L. Luxon, L.G. Davis, Fusion Technol. 8 (Part 2A) (1985) 441.
[24] J.G. Watkins, J. Salmonson, R. Moyer, et al., Rev. Sci. Instrum. 63 (10 Part 2) (1992) 4728.
[25] J.A. Boedo, D. Gray, M. Schaffer, et al., Rev. Sci. Instrum. 70 (7) (1999) 2997.
[26] L.L. Lao et al., Nucl. Fusion 25 (1985) 1611.
[27] G. McKee, R. Ashley, R. Durst, R. Fonck, et al., Rev. Sci. Instrum. 70 (1) (1999) 913.
[28] C. Fenzi, R.J. Fonck, M. Jakubowski, G.R. McKee, Rev. Sci. Instrum. 72 (1) (2001) 988.
[29] B. La Bombard, R. Boivin, M. Greenwald, et al., Phys. Plasmas 8 (5) (2001) 2107.
[30] D. Rudakov, J. Boedo, R. Moyer, et al., Rev. Sci. Instrum. 72 (1) (2001) 453.
[31] D. D'Ippolito, J. Myra, S. Krasheninnikov, Phys. Plasmas 9 (1) (2002) 222.
[32] S. Krasheninnikov, Phys. Lett. A 283 (2001) 368.